Local cell mechanics investigation by atomic force microscopy mapping and optical tweezers vertical indentation

G. Coceano,[ab] M.S. Yousafzai,[abc] W. Ma,[d] F. Ndoye,[ef] L. Venturelli,[abc] I. Hussain,[d] S. Bonin,[g] J. Niemela,[e] G. Scoles,[c] D. Cojoc[*a] and E. Ferrari[*d]

[a] CNR-IOM National Research Council - Institute of Materials, Area Science Park, Basovizza, S.S. 14, Km 163.5, 34149 Trieste, Italy.

[b] Università degli studi di Trieste, Piazzale Europa 1, 34128 Trieste, Italy.

[c] Dipartimento di Scienze Mediche e Biologiche, Università degli Studi di Udine, Piazzale Kolbe 4, 33100 Udine, Italy.

[d] University of Lincoln, Joseph Banks Laboratories, Green Lane, LN6 7DL Lincoln, UK.

[e] Abdus Salam International Centre for Theoretical Physics (ICTP), Strada Costiera 11, 34149 Trieste, Italy.

[f] Université Cheikh Anta Diop Dakar 5005, Sénégal.

[g] Dipartimento di Scienze Mediche Chirurgiche e della Salute, Università degli Studi di Trieste, Strada di Fiume 447, Ospedale di Cattinara, 34149 Trieste, Italy.

[*] Shared corresponding authorship:
D. Cojoc, Email: cojoc@iom.cnr.it;
E. Ferrari, Email: eferrari@lincoln.ac.uk

Abstract

The investigation of mechanical properties of cells represents a potential source of label free markers of cancer progression, based on measurable viscoelastic parameters. The Young modulus proved to be the most studied so far, however, even for the same cell type, the elastic modulus reported in different studies spans over a wide range of values, mainly due to the application of different experimental conditions. This complicates a reliable use of elasticity for mechanical phenotyping of cells. Here we combine two complementary techniques, Atomic Force Microscopy (AFM) and Optical Tweezers Microscopy (OTM), providing a comprehensive mechanical comparison of three human breast cell lines: normal myoepithelial (HBL-100), luminal breast cancer (MCF-7) and basal breast cancer (MDA-MB-231) cells. The elastic modulus was locally measured by AFM and OTM on single cells, using similar indentation approaches but different measurement parameters. Peak force tapping AFM was employed at nN forces and high loading rate to draw a viscoelastic map of each cell and the results indicated the region on top of the nuclei as the most meaningful. OTM was employed at those locations at pN forces and low loading rates, to measure the elastic modulus in a real elastic regime and rule out the contribution of viscous forces typical of AFM. When measured by either AFM or OTM, the cell lines elasticity trend was similar for the aggressive MDA-MB-231 cells, which were found to be significantly softer than the other two cell types in both measurements. However, when comparing HBL-100 and MCF-7 cells, we found significant differences only when using OTM.

Keywords

Cell Bio-mechanics, Breast Cancer, Atomic Force Microscopy, Optical Tweezers

Introduction

Cancer is a multifactorial disease and there is a general consensus in identifying the hallmarks that better describe the onset and progression of the disease [1, 2]. However, more recently, attention is growing on extra factors that characterise cancer: the mechanical changes that the tumour cells acquire and induce in the surrounding microenvironment [3-6]. While this aspect is especially evident at the tissue invasion and metastasis stage, the overall change in the mechanical properties of a tissue starts much earlier, involving several physiological processes that, by altering the membrane and cytoskeleton structure, convert a malignant cell into a metastatic one [5, 7]. It is known that cancer cells are softer and hence more deformable than non-tumour cells [8-10] and this eventually leads to their increased ability to infiltrate the tissues, spread from the primary tumour site and establish secondary sites [11].

Metastasis is the most common cause of death in breast cancer patients. In females, breast cancer is the most frequent tumour [12]. Therefore a thorough characterization of the mechanical properties of breast cancer cells would be beneficial for the understanding of the underlying molecular events that lead to metastasis [13] and could provide potential label-free markers based on mechanical measurements rather than molecular diagnostics [14].

Automated instruments capable to screen the elasticity of tissues from patients in a high-throughput fashion are still not available [15], however the community studying biomechanics at single-cell level can typically benefit, among others, from two robust biophysical techniques that have been developed and improved for few decades: Atomic Force Microscopy (AFM) and Optical Tweezers Microscopy (OTM).

AFM allows the imaging of living cells at high resolution in a liquid environment. An oscillating cantilever, driven by a piezoelectric actuator, indents the specimen along the Z vertical axis through a conical or spherical-shaped tip, mounted at the end of the cantilever (Fig. 1a). While oscillating along Z, the piezoelectric XY actuators perform a raster scan of the sample, typically covering all the area occupied by a single cell. During the raster-scan, the feedback loop system of the instrument collects the laser light reflected by the deflected cantilever on a four quadrant photo-detector and uses the voltage readouts to feed the Z piezoelectric actuator, correct the vertical position and generate a topographic image of the sample. Simultaneously, the instrument can convert the voltage signal acquired during each indentation event into displacement/force curves from which several mechanical properties, including elasticity, can be calculated, upon calibration of the detection system and the stiffness of the probe [16, 17].

Although AFM is not a high-throughput imaging technique, due to the mechanical nature of the interaction with the sample, it offers the unique opportunity to measure and map the local elasticity of a sample at high spatial resolution. For this reason, the technique has been extensively applied to the study of cancer cell biomechanics [18, 19]. The acquisition of robust datasets and the interpretation of the elasticity maps are often complicated by the fact that the mechanical interaction with soft-samples, such as living cells, can lead to membrane damage during the indentation, due to the sharpness of the tip (required for a high resolution image) and to the intensity of the force applied (typically in the nN

range). Beside this, the loading rate (the rate at which the force is vertically applied to the sample during the indentation) has to be relatively high to allow the acquisition of a representative area of the sample within a realistic time and before the living cell under investigation changes position or starts showing signs of distress beyond the control of the operator. To overcome these limitations and avoid cell damage, we opted to operate the AFM Z piezoelectric actuator with a sinusoidal waveform in peak force tapping mode (see Methods) [20].

At high loading rates, cells tend to respond to indentation also with a viscous component, which instead would be the only contribution when indenting at low loading rates [21-23]. Using OTM rather than AFM limits the loading rate and the indentation force, thus reducing the likelihood of rupture of the membranes and viscous responses to indentation. OTM relies on a spherical microprobe trapped by a highly focused laser beam. The displacement of the probe from the focus of the beam is linearly related to the external force by a constant, the trap stiffness. Since the probe confinement is non mechanical and the stiffness of the trap is typically very low and easy to fine tune, OTM probing is much more "gentle" than AFM. Indentation using an OTM trapped microbead (Fig. 1b) is achieved either by moving the trapping objective vertically [21] or by keeping the position of the laser focus fixed while the stage, where the cell-containing dish is clamped, approaches the bead by using a piezoelectric actuator along the Z vertical axis [23]. As soon as the cell membrane touches the microbead, this is displaced vertically, undergoing a force proportional to its displacement. The displacement of the probe is measured from the change of the interference pattern produced by the scattered laser beam by the microbead on a photo-diode [21] or a quadrant photo-detector [23]. Similarly to the case of the AFM, this signal can be converted into a displacement/force curve.

Opposite to AFM, OTM acquires curves only from single points rather than mapping the curves on a topographic image. This limitation is due to the large size of the probe that wouldn't allow high resolution mapping and especially to the low frequency at which the probe oscillates (in this study it was 0.2 Hz, compared to 0.25-0.5 kHz for the AFM), making the technique extremely time-consuming. Nevertheless, because of the high accuracy that OTM-obtained mechanical data can offer at low forces and the virtually ideal elastic conditions in which they can be acquired, OTM has been extensively used to characterise local mechanical properties of cells [24-27].

Using AFM and OTM vertical indentation we investigated locally the cell stiffness for three breast cancer cell lines: basal breast cancer cell line (MDA-MB-231), luminal breast cancer cells (MCF-7) and normal myoepithelial cells (HBL-100). Peak force tapping AFM allowed us to extract the viscoelastic map of the cell and define the region on the top of the nucleus as the most appropriate for reliable measurement. The cell indentation scheme used by AFM and OTM was similar, but the indentation forces and the loading rates were very different between AFM and OTM. This allowed us to observe the cell response at different mechanical regimes. The results in terms of cell stiffness were similar for MDA-MB-231 cell line, showing that these cells have the lowest stiffness. However, HBL-100 and MCF-7 showed different behavior when analyzed by AFM and OTM.
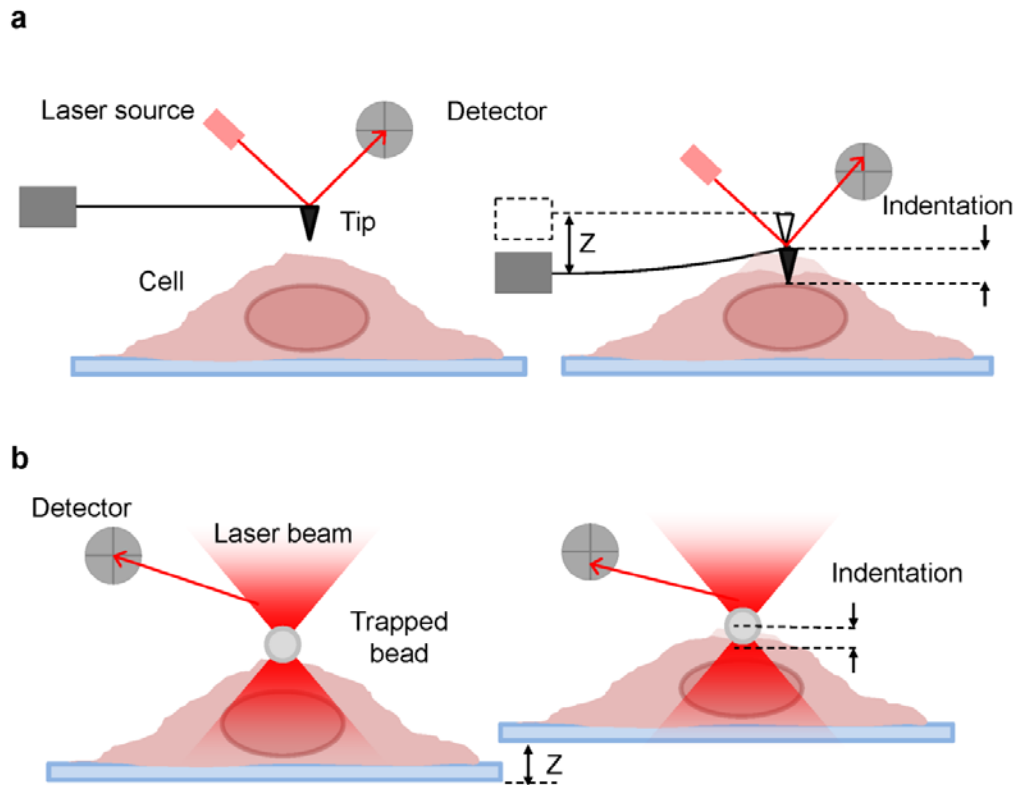
Figure 1. Vertical indentation of living cells. (a) In AFM, a cantilever driven by a piezoelectric actuator moves vertically along the Z axis. As the tip contacts the cell, the cantilever is deflected and the change in the laser reflection angle is recorded by a Quadrant Photo Detector (QPD). The indentation region corresponds to the part of vertical displacement for which a deflection of the cantilever can be observed. (b) In OTM, a laser-trapped bead is kept in a fixed position just above the cell while the piezoelectric stage holding the sample moves vertically. As the cell approaches and contacts the bead, this is displaced from the centre of the trap and the change of the interference pattern produced by the laser scattered by the bead is recorded by a QPD. The indentation region is defined as the portion of vertical displacement of the stage for which a displacement of the bead from the trap can be observed.

Methods

Cell cultures

MDA-MB-231, MCF-7 and HBL-100 cell lines (ATCC numbers HTB-26, HTB-22, HTB-124 respectively) were cultured in adhesion using low glucose Dulbecco's Modified Eagle Medium (DMEM) with L-glutamine (MDA-MB-231 and MCF-7) or Roswell Park Memorial Institute (RPMI) 1640 medium with L-glutamine (HBL-100), all supplemented with 10% (v/v) Fetal Calf Serum, 50 IU/ml of penicillin-streptomycin and 1mM gentamycin. Cell cultures were maintained in 25cm^2 flasks at 37°C in 5% CO_2. Cell splitting was performed every 2-3 days, as soon as the cultures reached the confluence, using 1:10 diluted 0.05% trypsin-EDTA. Cells were seeded overnight on 60mm polystyrene (AFM) or 30mm glass-bottom (OTM) Petri dishes at a density of 5×10^5 (AFM) or 2.5×10^5 (OTM) cells/ml in 6ml (AFM) or 2ml (OTM) of medium, washed three times in PBS and rinsed with medium prior to each measurement

session. All the reagents for cell culture were purchased from Gibco Life Technology, cell culture flasks and petri dishes were purchased from Sigma-Aldrich.

Atomic Force Microscopy

AFM imaging and indentation were performed on a BioScope Catalyst controlled by a NanoScope V controller (Bruker), combined with an Eclipse TE2000-S inverted optical microscope (Nikon) and equipped with a digital temperature controller unit (Lakeshore) to keep the cultured cells at 37°C during the acquisition of data. Images were acquired in Peak Force Quantitative Nanomechanical Mapping (PFQNM) mode [20] using DNP-10-A or ScanAsyst Fluid probes (Bruker), whose deflection sensitivity was determined by forcing their deflection on a glass surface and the spring constant (k) was estimated by the thermal tuning method (DNP-10-A nominal k=0.35N/m, ScanAsyst Fluid nominal k=0.7N/m). The nominal radius for tip and angles (same for both probe types), respectively 20nm and 15° (front)/25° (back)/17.5° (side), were used by the Nanoscope 9.0 software (Bruker) to compute the elastic modulus while scanning the images, using the Sneddon model for a conical indenter [28]. 128x128 or 256x256 points PFQNM images were acquired with a scan rate of 0.1-0.2Hz, a scan size of about 60μm (or the closest size that could accommodate the entire cell body), tapping amplitude of 750nm, frequency of 0.25-0.5kHz and a peak force set point of 1-2nN to avoid damaging the cell membranes while scanning. For each cell imaged, along with force/indentation curves for individual points, we recorded and analysed, using NanoScope Analysis 1.5 (Bruker), the following PFQNM channels: height, peak force, peak force error, adhesion, deformation, dissipation and Young's modulus.

Optical Tweezers Microscopy

A modular OTM (Thorlabs - OKBT) was adapted for axial cell indentation and force measurement [29]. Briefly, a collimated laser beam (YLM-5-IPG Photonics - Yb fiber laser 1064 nm) was focused through a 100X objective (Nikon, N.A.=1.25, oil immersion), to produce a stable optical trap for 3μm diameter silica microbeads (Bangs Laboratories) dispersed in the medium. During data acquisition, the cells were kept at 37°C by a temperature controller unit (RS Components) integrated into the setup. The sample was imaged through the trapping objective and a tube lens by a CMOS camera (Thorlabs - DCC1240C). A microbead probe was individually trapped and positioned above the cell nucleus area of a selected cell using a piezoelectric NanoMax 3-axis flexure stage (Thorlabs). The position of the microbead in the trap was tracked by back focal plane interferometry method [30] using the laser light scattered by the trapped bead. The trap height was in the range 3-6 μm from the cover slip. The trap stiffness was calculated using the equipartition theorem and the power spectrum density methods considering the stiffness variations due to spherical aberrations and neighbourhood of the cover slip [23]. Adjusting the laser power, trap stiffness was set to 0.015 pN/nm. To indent the cell, the stage on which the sample was clamped was moved vertically following a sinusoidal wave of 1 μm amplitude and 0.2 Hz frequency, while the laser focus was kept at a fixed position. The cell intercepted and interacted with the microbead in the second half of the sine period, thus causing a vertical displacement of the microbead with a proportional force (see Fig. S1).

Results and discussion

First, we used AFM to image representative cells from the three cultured lines, for the purpose of optimizing the parameters of the PFQNM while preserving the integrity and morphology of the cells. Fig. 2 shows that the cells are not damaged during the measurements. Besides the morphological information, given by the peak force error channel, the PFQNM technique simultaneously provided the Peak Force, Young's modulus, deformation, adhesion and dissipation maps (see Fig. S2 and Fig. S3).
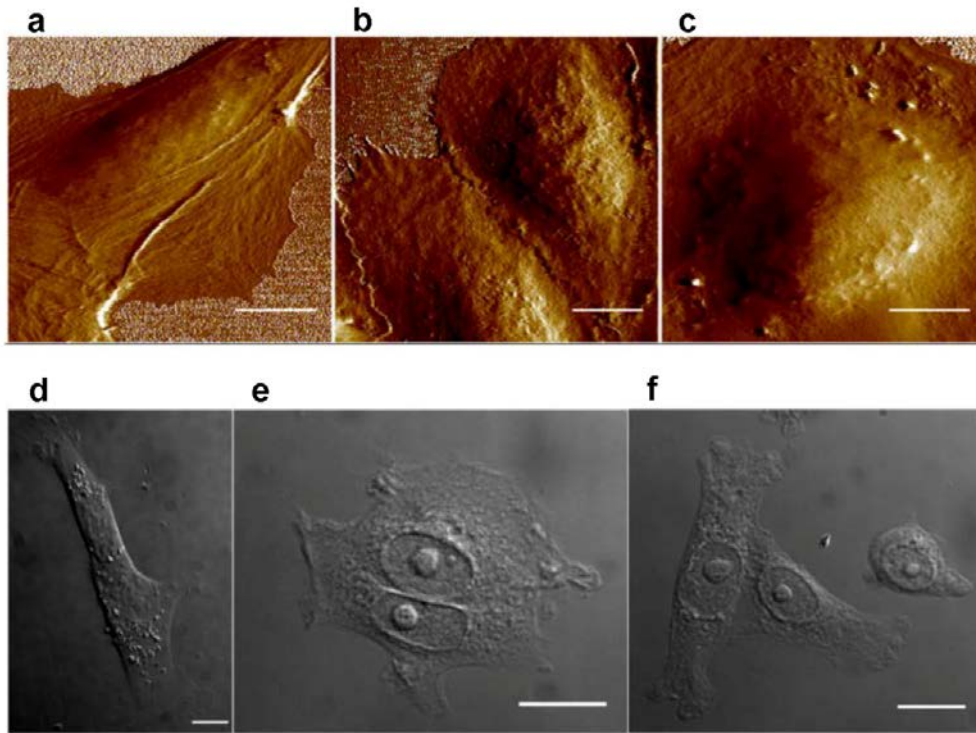
Figure 2. Morphology of the cells. The upper panels show AFM peak force error images of representative cells from the three cell lines analysed and the lower panels show DIC 90x optical images of cells from the same cultures: HBL-100 (a, d), MCF-7 (b, e) and MDA-MB-231 (c, f). All scalebars are 10μm. The peak force error channel output was chosen here to highlight the fine features in the images.

The Young's modulus (E) was mapped and calculated from the force (F)/indentation (δ) data acquired by AFM and automatically computed by the PFQNM package (Bruker) using the Sneddon model for a conical indenter (the tip) described by equation 1 [28].

$$E = \frac{\pi}{2}\frac{(1-\upsilon^2)}{\delta^2 \tan\alpha}F \qquad (1)$$

where υ is the Poisson ratio (0.4) and α the tip half angle (18°).

The OTM force (F)/indentation (δ) curves were analysed using a custom made Matlab (Mathworks) code and the computed Young's modulus was obtained, according to the Hertz model for a spherical indenter (the microbead), from equation 2 [21].

$$E = \frac{3}{4} \frac{(1-\upsilon^2)}{\delta \sqrt{r \cdot \delta}} F \qquad (2)$$

where r is the microbead radius (1.5 µm).

Fig. 3 shows representative experimental curves of force versus probe-sample separation, obtained during the interaction of the cell with the tip in AFM and the bead in OTM. Cell-probe interaction includes two phases: indentation (black trace in Fig. 3) and retraction (red trace). The difference between the indentation and retraction curves in Fig. 3a indicates dissipation due to viscoelastic behaviour of the cell at forces and loading rates specific to AFM. The indentation and retraction curves for OTM are instead almost identical (Fig. 3b), indicating that the cell response to lower forces is entirely elastic. While the elasticity data from the OTM analysis were the result of a Hertz fit (equation 2) on individual indentation event, the elastic modulus from AFM measurements was computed automatically by the acquisition software using a Sneddon fit (equation 1) like the one shown in Fig. 3a for each point of the image and then averaged within a 2.5x2.5 µm square.
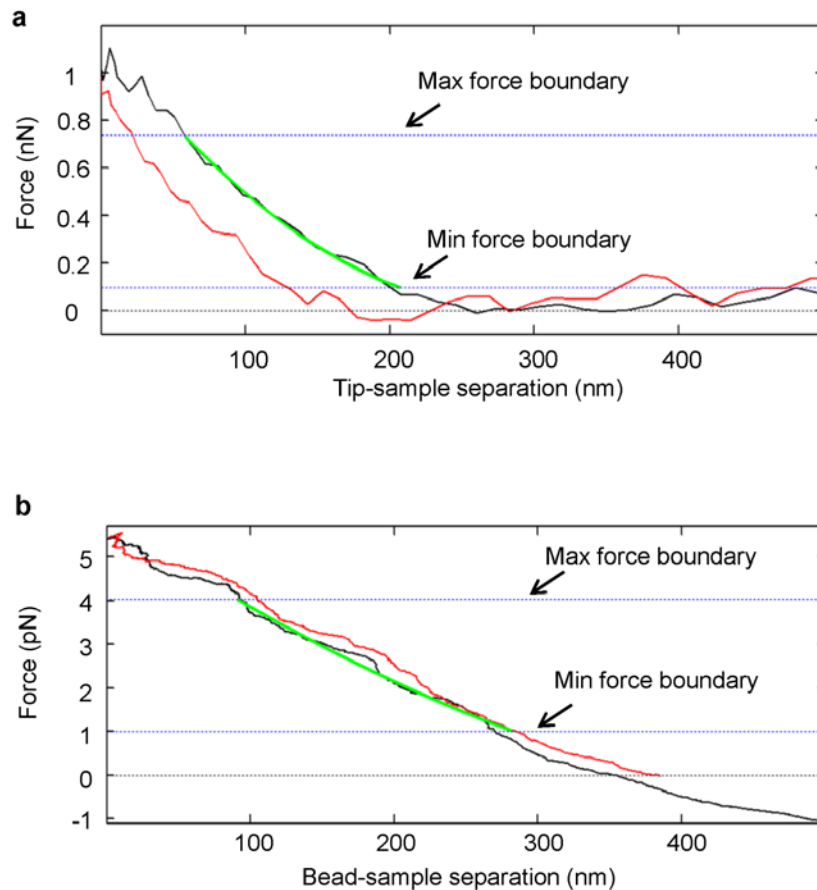

Figure 3. Force-separation curves of a representative indentation event on a MDA-MB-231 cell using AFM (a) and OTM (b). The plots show the indentation (black), retraction (red) experimental traces and the fitted curves (green) used to calculate the Young's modulus. Sneddon fit was used for AFM indentation (a) and Hertz fit for OTM (b). The fit is applied in a range of forces within min and max force boundaries.

Besides the Young's modulus, in AFM-PFQNM we analysed also other mechanical properties. The deformation channel was monitored to set indentations at about 200nm, sufficient for acquiring good elasticity data without damaging the cell membrane. The adhesion channel was also considered and used to rule out unusual adhesion values, that could have been the result of the formation of membrane tethers. The dissipation was considered to evaluate whether some areas of a cell were presenting a viscous behaviour that accounts for the loss of energy while indenting. To match all the conditions above, we established the optimal peak force set point in the range of 1-2nN and we consistently used this range for all the experiments on all the three cell lines.

We then analysed the distribution of the Young's modulus (Sneddon fit) on different areas of a representative AFM-imaged HBL-100 cell (Fig. 4). Data from the Young's modulus channel were avereged over small squares (2.5x2.5μm). The first square (labelled as 1 in Fig. 4a) was located above the nuclear area and other five squares were located at increasing distances, between the nuclear area and the leading edge of the cell. As evidenced by the data plotted in Fig. 4b and the corresponding values reported in Table 1, the Young's modulus decreases with the distance from the nuclear area.
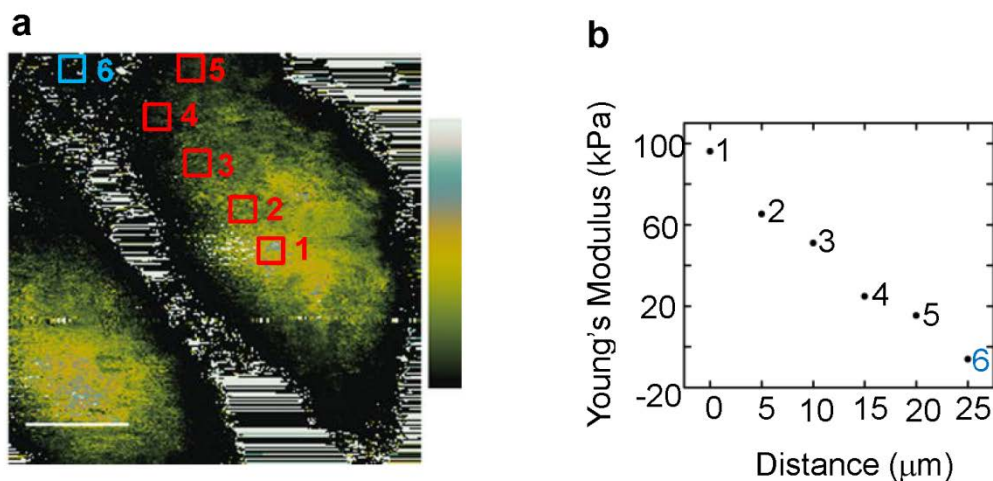
Figure 4. Distribution of the measured areas on a representative HBL-100 cell. (a) Location of the 6 2.5x2.5μm squares from which the Young's modulus has been calculated (AFM Sneddon channel, colorbar 0-300 kPa). The blue square identifies a position very close to the polystyrene substrate, which is too rigid to be indented and therefore does not show a realistic elastic module. The position of the nuclear area (square 1) has been estimated from the topography of the cell and corresponds to the position of the highest feature in the height channel. Scalebar is 10μm. (b) The mean values calculated from the squares in panel (a) plotted against the distance from the nuclear area.

| Position in Fig. 4	Distance from nuclear area (µm)	Young's modulus (kPa) (mean± SD)
1	0	96.1 ± 1.3
2	5	65.3 ± 0.7
3	10	51.0 ± 0.5
4	15	24.9 ± 1.2
5	20	15.4 ± 1.0
6	25	N.A.

Table 1. Young's modulus measured at different distances from the cell nucleus of a HBL-100 cell. The Young's modulus is expressed as the mean ± the standard deviation (SD) of the values included in the relevant squares of Fig. 4a (10x10 measuring points). As explained in the text, the value for position 6, 25µm away from the nucleus, is not measurable.

It is known that, due to the conical shape of the tip, the actual values of the Young's modulus at the periphery of the cells are overestimated [31]. Using the bottom effect cone correction, we found an overestimation of up to 30% at the periphery, where the cell height is less than 1 µm (see Table S1). Note that the square labelled 6 in Fig. 4a was deliberately chosen on the very edge of the cell to emphasise that the proximity of the substrate on which the cell adheres makes the elasticity measurement impractical. In fact, when the cell height is extremely low, the tip interacts with the substrate rather than the cell, making its deformation irrelevant in this area (see deformation maps in Fig. S3)

The trend of the elasticity modulus over the cell was examined for 22-30 individual cells of all three cell lines, by measuring the Young's modulus in three locations corresponding to the regions labeled 1 (nucleus), 3 (intermediate) and 5 (leading edge) on the representative HBL-100 cell shown in Fig. 4. As one can see from Table 2 and the barchart of Fig. 5, the Young's modulus decreases with the distance from the nucleus for all the three cell lines. These results confirm previous microrheology studies which have demonstrated a higher viscoelastic modulus for the nucleoplasm relative to cytoplasm, arising primarily due to the heterogeneous chromatin organization [32-34]. Altogether these findings suggest that the area on the top of the nucleus, where the Young's modulus is maximum, is the most meaningful for cell mechanics characterization.

	HBL-100		MCF-7		MDA-MB-231	
	Young's modulus (kPa)	n	Young's modulus (kPa)	n	Young's modulus (kPa)	n
Nuclear area	95.4 ± 43.6	30	87.3 ± 47.8	30	55.6 ± 20.1	22
Intermediate	63 ± 29.5	30	79.4 ± 51.8	30	37.4 ± 21.7	22
Leading edge	36.1 ± 18.4	30	50.2 ± 38.5	30	28.7 26.1	22

Table 2. Young's modulus values (mean ± standard deviation SD for n cells) measured in three different regions of the cell chosen in the same way as the squared regions 1, 3 and 5 shown in Fig. 4.
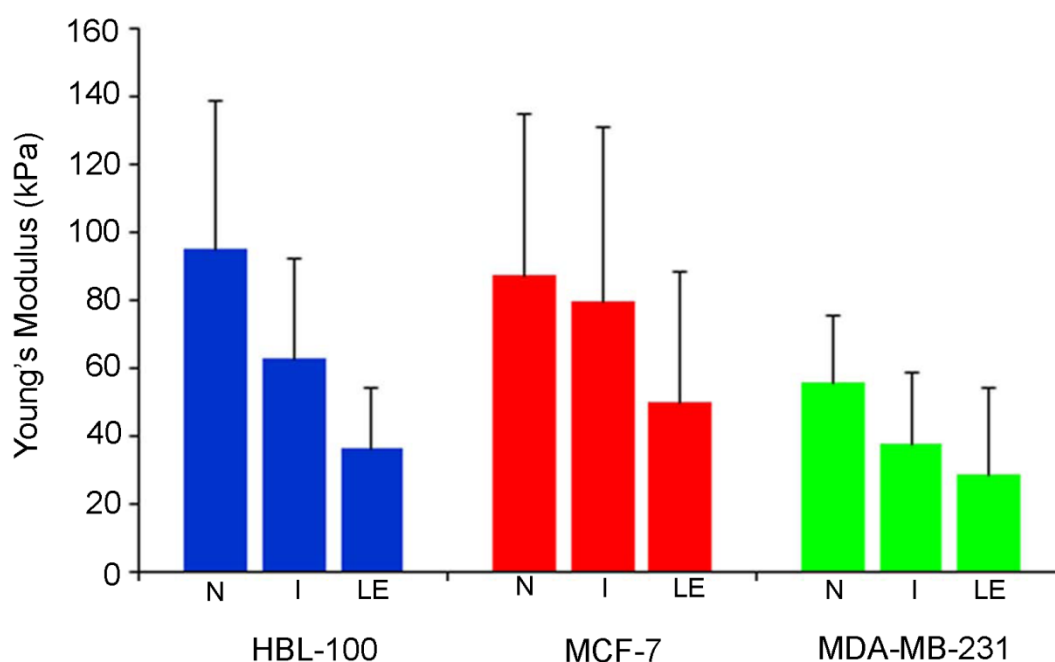
Figure 5. Young's modulus decreases with the distance from the nucleus. The barchart is a graphical representation of the data in Table 2. N- nuclear area, I- intermediate, and LE - leading edge.

Elasticity measurements on the top of the nucleus were systematically carried out also by OTM, on 22-32 single cells of each of the three cell lines. Nevertheless, we also verified that the Young's modulus was lower out of the nuclear region, measuring it in two-three points, arbitrarily chosen between the nuclear area and the leading edge, for ten cells of each cell line (data not shown). A typical image of a trapped bead positioned on the nucleus area of the cell for subsequent indentation is shown in Fig. 6.
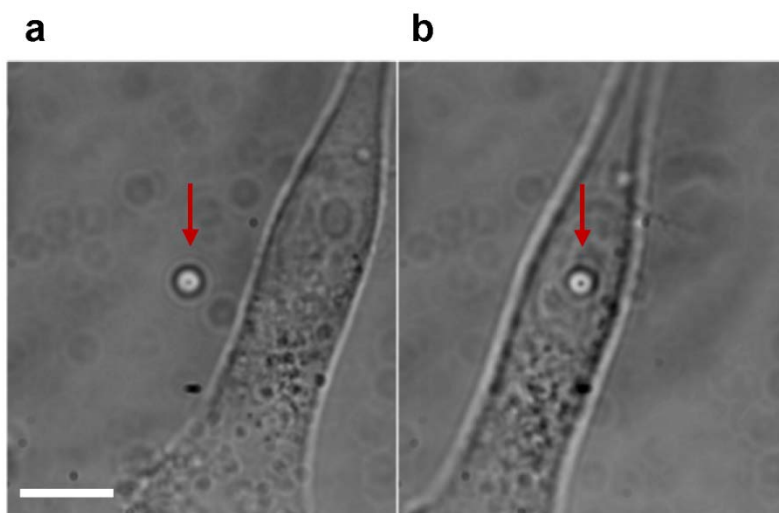
Figure 6. Optical images acquired by the OTM setup of a representative MDA-MB-231 cell, while a 3µm bead, highlighted by the red arrow, is trapped by the laser in the centre of the field of view (a) and positioned on the measuring area just above the nucleus by moving the stage (b). Scalebar is 10µm.

The Young's modulus values obtained by OTM (Table 3 and Fig. 7b) were several orders of magnitude lower than the AFM measurements on the same type of cells. This is due to differences in the indentation regimes used by OTM and AFM. Parameters as the loading rate, indentation force, probe stiffness, are all known to affect the measured value of Young's modulus [35, 36]. The low loading rate employed by OTM is a consequence of the lower forces exerted, but also of the low frequency at which the indenting oscillation happens (0.2Hz compared to 0.25-0.5kHz of the AFM tapping).

To compare the Young's modulus of the three different cell lines on the area of the nucleus by using both AFM and OTM, we summarised the data collected in Table 3 and graphically represented them in Fig. 7. The differences between the cell lines were calculated using the two tailed Mann-Whitney test (Minitab Statistical Software version 17). Although the mean values of the elastic modulus measured by OTM were always much lower than the one obtained by AFM indentation, the cell lines comparison showed the same important result: the basal breast cancer cell line MDA-MB-231 had a significantly lower Young's modulus than the other two, regardless of the technique and loading rate applied for the measurement. However, AFM and OTM gave different results when comparing the HBL-100 and MCF-7 cell lines. The difference between the elastic modulus of the HBL-100 and MCF-7 cell lines is not statistically significant ($p = 0.5$) when measured by AFM but the elasticity of MCF-7 becomes significantly higher than HBL-100 ($p < 0.05$) when measured by OTM. The discrepancy in the estimation of the cell type-specific elasticity when measured by AFM and OTM might be due to the fact that AFM force regimes are prone to originate inelastic responses. Therefore the measurements and the resulting statistics reported in Table 3 and Fig. 7 for OTM, might be more accurate than AFM, where viscous effects result in dissipation and compromise the measurement of the Young's modulus.

	AFM indentation		OTM indentation	
	Young's modulus (kPa)	n	Young's modulus (Pa)	n
HBL-100	95.4 ± 43.6	30	23.5 ± 10.6	32
MCF-7	87.3 ± 47.8	30	30.2 ± 15.0	32
MDA-MB-231	55.6 ± 20.1	22	12.6 ± 6.1	22

Table 3. Young's modulus measured by AFM and OTM indentation on the top of nucleus. The values represent mean ± the standard deviation (SD) over n cells.
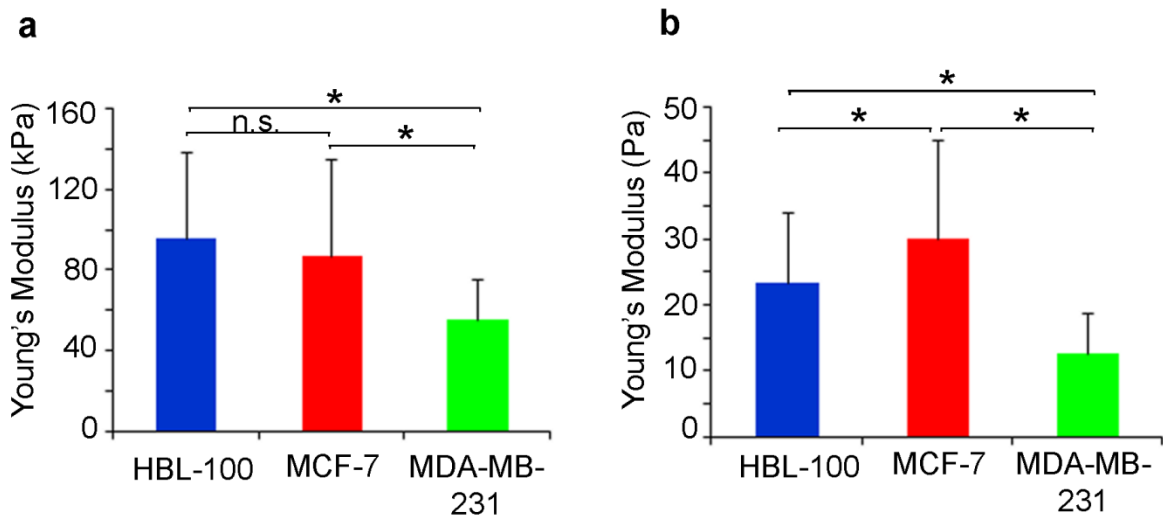
Figure 7. Graphical representation and statistical analysis of the data in Table 3. The Young's modulus of MDA-MB-231 is significantly lower (*P: <0.05) than the other two cell lines, both in AFM (a) and OTM (b) measurements. The difference between HBL-100 and MCF-7 is not significant (n.s.) in the AFM dataset, whereas for OTM it is (*P: <0.05).

To verify whether the undesirable viscous contribution in AFM is homogenously distributed across the cell, we used the dissipation channel measurements. By calculating the mean dissipation over small square areas, similarly to the Young's modulus calculation for the HBL-100 cell in Fig. 4, we observed larger dissipation values (more negative) for the nuclear area compared to the periphery (Fig. 8 and Table 4).
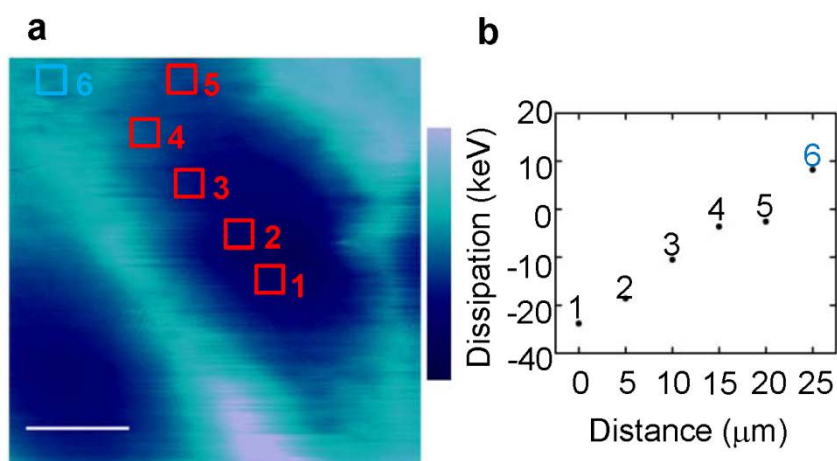
Figure 8. Dissipation measurements on different areas of a cell. (a) Dissipation map of the HBL-100 cell of Fig. 4. Colorbar -35-35 keV, Scalebar 10µm. (b) Mean values of dissipation for each of the 2.5x2.5µm squares plotted against the distance from the nuclear area, calculated as explained in Fig. 4. This map shows that the dissipation, due to viscosity, is primarily localised in the central area rather than the periphery. The viscous components of the cell evidenced here by AFM were not visible at OTM loading rate and stiffness regimes (see the overlapping indentation and retraction curves of Figure 3b).

Position in Fig. 8	Distance from nuclear area (µm)	Dissipation (keV) ± SD
1	0	-23.8 ± 0.1
2	5	-18.6 ± 0.2
3	10	-10.5 ± 0.2
4	15	-3.6 ± 0.1
5	20	-2.6 ± 0.1
6	25	N.A.

Table 4. Dissipation measured at different distances from the cell nucleus of the representative HBL-100 cell of Fig. 8. The dissipation is expressed as mean values for each square (10x10 pixels) ± the standard deviation (SD). The value for position 6, 25µm away from the nuclear area, is not measurable because it is too close to the non-deformable substrate.

These results suggest that the thickness of the cell body contribute to the stronger viscous effects in the nuclear region, while near the periphery, where the cell is thinner, the effect tends to be negligible. This suggests that measuring the Young's modulus away from the nuclear area could be beneficial [37]. However, we pointed out earlier that the relative differences between cell lines' elasticity are more evident when this is measured near the nucleus (Fig. 5) and the overestimation of the modulus due to the tip conical shape is less dramatic (Table S1). Moreover, depending on the morphology of the specific cell line under analysis, the periphery of the adherent cells can potentially be very different and difficult to standardise across cell types, while the nuclear area tend to be morphologically more consistent, even in the case of highly polarised cells, thus facilitating a direct comparison between cell types. Overall, this study shows that AFM elasticity measurements on the nuclear area represent the best option to mechanically compare different cell lines, however, due to the uneven dissipation within a single cell body, elasticity maps could provide useful extra information that are dependent on the unique morphology of the sample. We envisage this would be of particular importance in the case of other highly polarised cells, like for example neurons.

Moreover, our approach compensates the potential inaccuracy of AFM in the estimation of the Young's modulus at the nuclear area by acquiring a second set of data by OTM under near-ideal elastic conditions. In fact we observed that the viscous components in OTM measurements was negligible as evidenced by the fact that the indentation and retraction curves of Fig. 3b almost overlap, showing that there is virtually no dissipation during the slow and "gentle" indentation process.

Conclusions

We described an integrated approach for the quantitative analysis of elasticity data from single cells, using two complementary techniques: AFM and OTM indentation. The study on three breast cell lines reported here, conclusively shows that basal breast cancer cells (MDA-MB-231) are softer than their normal counterpart (myoepithelial HBL-100) and the less aggressive luminal breast cancer cell line (MCF-7), reflecting their aggressiveness and thus their potential infiltrating nature that could lead to metastasis. These findings, obtained both with AFM and OTM are in line with previous studies [22, 35, 38]. We proved that it is possible to non-destructively image and map the Young's modulus by the use of a recently introduced AFM imaging mode, the Peak Force Quantitative Nanomechanical Mapping (PFQNM), and we optimized the parameters to obtain consistent data within a realistic time for live imaging. We observed that the elasticity is not homogeneously distributed across cells, and we identified the area just above the nucleus as the most accessible for determining elasticity differences between cell lines. We also identified and mapped the contribution of viscous forces on the cell body and we found that AFM tends to have larger dissipation on the region of the nuclear area. We correlated this with the loading rate of the technique used, concluding that, although mapping would be unrealistic, OTM is a preferable technique, as it allows measuring mechanical properties of cells in a nearly ideal elastic manner. We evidenced that for some cell lines, as it was the case of the comparison between MCF-7 and HBL-100, the elasticity measurements can give different results when using AFM or OTM, highlighting the importance of an integrated approach and a careful interpretation of the findings.

The set of techniques described here and the conclusions drawn contribute to the broader and systematic understanding of cancer biomechanics and to the ultimate goal of assessing the potential of cells to lead to metastasis by considering mechanical clues rather than molecular markers only. The biological insight that can be obtained from here is that determining visco-elastic parameters at sub-cellular resolution using the approach described could be used as an indicator of metastasis, based on the significant differences observed on the metastatic model MDA-MB-231 in comparison to less aggressive cells. We also envisage that this approach could be suitable for high-resolution mapping of visco-elastic parameters of soft materials other than living cells, for example PFQNM could be used to characterise and map nanostructured scaffolds for tissue engineering and OTM applied to probe the material at selected locations.

Competing interests

We have no competing interests.

Authors' contribution

GC and WM performed atomic force microscopy; MSY and FN performed optical tweezers; GC, LV, IH and SB carried on cell culture; MSY, FN, JN and DC contributed to the development of the optical tweezers custom setup; GC, MSY, FN, DC and EF analysed the experimental data; LV performed optical microscopy; GC, SB, JN, DC and EF contributed to the conception and design of the study; GC, DC and EF wrote the manuscript; GS and SB critically supported the drafting of the manuscript with substantial intellectual content and interpretation of the data.

Funding

References

1. Hanahan D, Weinberg RA 2000 The hallmarks of cancer *Cell* **100** 57–70
2. Hanahan D, Weinberg Robert A 2011 Hallmarks of Cancer: The Next Generation *Cell* **144** 646-674
3. Mierke CT 2014 The fundamental role of mechanical properties in the progression of cancer disease and inflammation *Rep. Prog. Phys.* **77** 076602
4. Ketene AN, Schmelz EM, Roberts PC, Agah M 2012 The effects of cancer progression on the viscoelasticity of ovarian cell cytoskeleton structures *Nanomed. Nanotechnol. Biol. Med.* **8** 93-102
5. Plodinec M, Loparic M, Monnier CA, Obermann EC, Zanetti-Dallenbach R, Oertle P, Hyotyla JT, Aebi U, Bentires-Alj M, Lim RYH*, et al.* 2012 The nanomechanical signature of breast cancer *Nat. Nanotechnology* **7** 757-765
6. Venugopalan G, Camarillo DB, Webster KD, Reber CD, Sethian JA, Weaver VM, Fletcher DA, El-Samad H, Rycroft CH 2014 Multicellular architecture of malignant breast epithelia influences mechanics *PLoS ONE* **9**

7. Costa KD 2004 Single-cell elastography: probing for disease with the atomic force microscope *Dis. Markers* **19** 139–154

8. Sugawara Y, Ando R, Kamioka H, Ishihara Y, Murshid SA, Hashimoto K, Kataoka N, Tsujioka K, Kajiya F, Yamashiro T*, et al.* 2008 The alteration of a mechanical property of bone cells during the process of changing from osteoblasts to osteocytes *Bone* **43** 19-24

9. Guck J, Schinkinger S, Lincoln B, Wottawah F, Ebert S, Romeyke M, Lenz D, Erickson HM, Ananthakrishnan R, Mitchell D*, et al.* 2005 Optical Deformability as an Inherent Cell Marker for Testing Malignant Transformation and Metastatic Competence *Biophysical Journal* **88** 3689-3698

10. Rother J, Nöding H, Mey I, Janshoff A 2014 Atomic force microscopy-based microrheology reveals significant differences in the viscoelastic response between malign and benign cell lines *Open Biology* **4**

11. Lekka M, Pogoda K, Gostek J, Klymenko O, Prauzner-Bechcicki S, Wiltowska-Zuber J, Jaczewska J, Lekki J, Stachura Z 2012 Cancer cell recognition - Mechanical phenotype *Micron* **43** 1259-1266

12. Parkin DM, Bray F, Ferlay J, Pisani P 2001 Estimating the world cancer burden: Globocan 2000 *Int. J. Cancer* **94** 153-156

13. Cross SE, Jin Y-S, Rao J, Gimzewski JK 2007 Nanomechanical analysis of cells from cancer patients *Nat. Nanotechnology* **2** 780-783

14. Cross SE, Jin Y-S, Tondre J, Wong R, Rao J, Gimzewski JK 2008 AFM-based analysis of human metastatic cancer cells *Nanotechnology* **19** 384003

15. Di Carlo D 2012 A Mechanical Biomarker of Cell State in Medicine *J. Lab. Autom.* **17** 32-42

16. Müller DJ, Dufrene YF 2008 Atomic force microscopy as a multifunctional molecular toolbox in nanobiotechnology *Nature Immunology* **3** 261–269

17. Harris AR 2011 Experimental validation of atomic force microscopy-based cell elasticity measurements *Nanotechnology* **22** 345102

18. Lekka M, Laidler P, Gil D, Lekki J, Stachura Z, Hrynkiewicz AZ 1999 Elasticity of normal and cancerous human bladder cells studied by scanning force microscopy *Eur. Biophys. J.* **28** 312-316

19. Lee GYH, Lim CT 2007 Biomechanics approaches to studying human diseases *Trends Biotechnol.* **25** 111-118

20. Pittenger B, Erina N, Su C 2010 Quantitative mechanical property mapping at the nanoscale with PeakForce QNM *Application Note #84 Veeco Instruments Inc*

21. Nawaz S, Sánchez P, Bodensiek K, Li S, Simons M, Schaap IAT 2012 Cell Visco-Elasticity Measured with AFM and Optical Trapping at Sub-Micrometer Deformations *PLoS ONE* **7** e45297

22. Li QS, Lee GYH, Ong CN, Lim CT 2008 AFM indentation study of breast cancer cells *Biochem. Biophys. Res. Commun.* **374** 609-613

23. Bodensiek K, Li WX, Sanchez P, Nawaz S, Schaap IAT 2013 A high-speed vertical optical trap for the mechanical testing of living cells at piconewton forces *Rev. Sci. Instrum.* **84** 113707

24. Hong-Lian G, Chun-Xiang L, Jian-Fa D, Yu-Qiang J, Xue-Hai H, Zhao-Lin L, Bing-Ying C, Dao-Zhong Z 2004 Mechanical Properties of Breast Cancer Cell Membrane Studied with Optical Tweezers *Chinese Phys. Lett.* **21** 2543

25. Tavano F, Bonin S, Pinato G, Stanta G, Cojoc D 2011 Custom-Built Optical Tweezers for Locally Probing the Viscoelastic Properties of Cancer Cells *Int. J. Optomechatronics* **5** 234-248

26. Titushkin I, Cho M 2006 Distinct Membrane Mechanical Properties of Human Mesenchymal Stem Cells Determined Using Laser Optical Tweezers *Biophys. J.* **90** 2582-2591

27. Sheetz MP, Dai J 1996 Modulation of membrane dynamics and cell motility by membrane tension *Trends Cell Biol.* **6** 85-89

28. Sneddon IN. 1951 *Fourier Transforms*. McGraw-Hill.

29. Yousafzai MS, Ndoye F, Coceano G, Niemela J, Bonin S, Scoles G, Cojoc D 2015 Substrate-dependent cell elasticity measured by optical tweezers indentation *Optics and Lasers in Engineering* **http://dx.doi.org/10.1016/j.optlaseng.2015.02.008**

30. Gittes F, Schmidt CF 1998 Interference model for back-focal-plane displacement detection in optical tweezers *Opt. Lett,* **23** 7-9

31. Gavara N, Chadwick RS 2012 Determination of the elastic moduli of thin samples and adherent cells using conical atomic force microscope tips *Nature Nanotechnology* **7** 733-736

32. Geiger B, Spatz JP, Bershadsky AD 2009 Environmental sensing through focal adhesions *Nature Reviews: Molecular Cell Biology* **10** 21-33

33. Simon DN, Wilson KL 2011 The nucleoskeleton as a genome-associated dynamic 'network of networks' *Nature Reviews: Molecular Cell Biology* **12** 695-708

34. Aebi U, Cohn J, Buhle L, Gerace L 1986 The nuclear lamina is a meshwork of intermediate-type filaments *Nature* **323** 560-564

35. Chiou Y-W, Lin H-K, Tang M-J, Lin H-H, Yeh M-L 2013 The Influence of Physical and Physiological Cues on Atomic Force Microscopy-Based Cell Stiffness Assessment *PLoS ONE* **8** e77384

36. Alcaraz J, Buscemi L, Grabulosa M, Trepat X, Fabry B, Farré R, Navajas D 2003 Microrheology of Human Lung Epithelial Cells Measured by Atomic Force Microscopy *Biophys. J.* **84** 2071-2079

37. Berquand A, Holloschi A, Trendelenburg M, Kioschis P 2010 Analysis of Cytoskeleton-Destabilizing Agents by Optimized Optical Navigation and AFM Force Measurements *Micros. Today* **18** 34

38. Leporatti S, Vergara D, Zacheo A, Vergaro V, Maruccio G, Cingolani R, Rinaldi R 2009 Cytomechanical and topological investigation of MCF-7 cells by scanning force microscopy *Nanotechnology* **20** 055103